Electromagnetic bubbles: subcycle near-femtosecond and subfemtosecond field solitons

A. E. Kaplan, S. F. Straub, and P. L. Shkolnikov

Department of Electrical and Computer Engineering, The Johns Hopkins University, Baltimore, Maryland 21218

Received February 26, 1997; revised manuscript received March 31, 1997

We demonstrate the feasibility of strong (up to atomic fields) and supershort (few-femtosecond or even subfemtosecond) subcycle (nonoscillating) electromagnetic solitons [EM bubbles (EMB's)] in a gas of two-level atoms as well as EMB's and preionization shock waves in classically nonlinear atoms. We show that EMB's can be generated by existing sources of radiation, including subpicosecond half-cycle pulses and short laser pulses. We investigate how EMB characteristics are controlled by those of originating pulses. Our most recent results are focused on related transient phenomena, including EMB formation length, multibubble generation, and shocklike waves. © 1997 Optical Society of America [S0740-3224(97)03011-7]

1. INTRODUCTION

Contemporary optics usually operates with almost harmonic, multicycle oscillations modulated by an envelope much longer than a single cycle of the oscillations. In fact, any narrow-line radiation is an envelope signal, be it a coherent radiation of a laser or an incoherent light filtered through a spectroanalyzer. This is also true for any optical pulse, including self-induced transparency solitons in two-level systems[1] (TLS's) described by Maxwell–Bloch or sine-Gordon equations, mode-locked laser pulses[2] owing to multimode cavity interaction with a laser medium, and optical-fiber solitons[3] owing to Kerr nonlinearity described by a nonlinear Schrödinger equation.[4] To describe any of those pulses, slowly varying envelope approximations are used in both the propagation (by reduction of Maxwell equations to a parabolic partial differential equation) and the material response (rotating-wave approximation in constitutive equations). Because of the availability of very short laser pulses (down to ~6-fs length[5]) with just a few laser cycles, efforts are made to improve the envelope approximation at least for linear propagation (see, e.g., Ref. 6).

Many new experimental techniques and applications, however, such as time-domain spectroscopy[7] of dielectrics, semiconductors, and flames[8] and of transient chemical processes such as dissociation and autoionization[9]; new principles of imaging[10]; and atomic physics by means of photoionization[11] would greatly benefit from the availability of short and intense electromagnetic pulses of a nonoscillating nature, i.e., subcycle (almost unipolar) half-cycle pulses (HCP's). The spectra of currently available HCP's generated in semiconductors by means of optical rectification reach into the terahertz domain; these HCP's are ~400–500 fs long, with a peak field of 150–200 kV/cm.[9]

Recently[12,13] we proposed two new principles of generating much shorter (down to 0.1 fs $= 10^{-16}$ s) and stronger (up to $\sim 10^{16}$ W/cm^2) pulses. One of these principles is based on stimulated cascade Raman scattering[12] and results in the generation of an almost periodic train of powerful subfemtosecond pulses, whereas the other relies on the generation of powerful electromagnetic bubbles[13] (EMB's), which are subcycle solitary pulses of EM radiation propagating in a gas of two-level or classically nonlinear atoms. The latter effect would allow one to generate a single EMB, or a few EMB's with controllable parameters, each EMB propagating with a different velocity such that one can easily separate the EMB's into individual pulses. In this paper we review our recent research on EMB's and present new related results on transient processes, in particular, on the formation length of EMB's, the generation of multi-EMB's, and the formation of shock and shocklike waves.

Such supershort and intense subcycle pulses might be of great interest for a host of applications (see below). Especially significant are nonoscillating solitary waves able to propagate over substantial distances with unchanged shape and length. The exact solitonlike solutions for the nonlinear propagation of unipolar pulses in the strongly driven TLS described by full Maxwell–full Bloch equations, were found quite a while ago.[14] The solutions have a familiar, 1/cosh, profile, with its duration and velocity related to its amplitude. At that time the authors of Ref. 14 did not believe that such nonlinear pulses were feasible; the main stumbling point that they saw was that the pulse intensities would exceed $\sim 10^{14}$ W/cm^2, a level inaccessible then. Now optical fields a few orders of magnitude larger are available; however, one of the major problems in the generation of such short (and intense) pulses is that the TLS model used in the theory[14] (and in some more-recent research[15,16]) will be stretched far beyond its limitations because intensities above $\sim 10^{14}$ W/cm^2 cause fast over-the-barrier ionization. What are the largest intensities (and thus the shortest lengths) of these pulses that can still be supported by atomic gases? What are new properties of these pulses

0740-3224/97/113013-12$10.00

beyond the TLS approximation? Fortunately, these and other questions about high-intensity supershort pulses can be addressed by use of the very fact that the atom is so strongly excited that one can use again its classical (as opposed to quantum) description.[13] In the intermediate domain, a multilevel quantum approach has to be used.

We show here that EMB's are not only feasible but natural for many nonlinear systems, both quantum and classical. Their length may range from picoseconds to subfemtoseconds, depending on their intensity. We call them electromagnetic bubbles to stress their nonenvelope nature. We demonstrate that field ionization, a fundamental factor not considered previously, imposes an upper limit on the amplitude of the EMB and a lower limit on its length; after an EMB reaches its shortest length at some peak amplitude, further increase of the amplitude results in EMB broadening. At some threshold amplitude, the EMB degenerates into a shock wave that is a precursor of a dc ionizing field—a new feature that is not present in the TLS model. Furthermore, we show that even at much lower peak intensities, when the TLS model may still be valid, the initially smooth HCP may drastically steepen to form a shocklike wave that then breaks in a multi-EMB solution.[17] Unlike a dc ionization precursor shock wave, this shocklike wave can appear far below the ionization.

EMB's can be as short as 10–0.1 fs, with amplitudes approaching the atomic field. These supershort and intense subcycle pulses might be of great interest for a host of applications. They can be used for a global spectroscopic technique based on a shocklike excitation across the entire atomic spectrum (to an extent similar to that of passing atoms through a foil), including normally prohibited transitions. The ionization by a pulse shorter than the orbital period may bridge a gap between conventional photoionization and collisional ionization by a particle,[11] with the important difference being that EM pulses offer a control of the quantum state of the atom during the entire process and hence a control of the atom's final state. This control, in turn, has far-reaching implications for applications in time-resolved spectroscopy of transient chemical processes such as dissociation and autoionization that occur on a femtosecond time scale (see, e.g., Ref. 9), especially for quantum control of chemical transformations (see, e.g., Ref. 18). These new pulses may expand time-domain spectroscopy of dielectrics, semiconductors, and flames[8] from the currently available terahertz domain[7–11] to optical frequencies. One can also envisage their applications to probing high-density plasmas, testing the speed of light, and imaging molecules and atoms at surfaces and for an order-of-magnitude frequency upconversion owing to the large Doppler shift of a counterpropagating coherent light backscattered by EMB's, etc. A train of subfemtosecond pulses with a very high repetition rate (~125 THz or with the spacing ~8 fs), which is feasible in cascade stimulated Raman scattering,[12] can be used for the stroboscopy of atomic motion in a molecule (for example, during its dissociation).

Another property of EMB's that may greatly facilitate their application is their extremely broad spectrum, which ranges from radio frequencies to the visible or even ultraviolet domain. A single pulse of such a nature would have a continuous power spectrum from zero frequency to the highest (cutoff) frequency of the pulse:

$$\omega_{\mathrm{cut}} \sim 2.6 t_p^{-1}, \tag{1.1}$$

where t_p is the pulse duration (evaluated at half-intensity). For example, with $\tau = 0.2$ fs, the cutoff wavelength, $\lambda_{\mathrm{cut}} = 2\pi c/\omega_{\mathrm{cut}} \sim 2.4 c t_p$, is ~144 nm, i.e., in the far ultraviolet. It would be seen by a human eye as an extremely short and powerful burst of white light. Even the spectrum of a much longer, 1-fs pulse, with $\lambda_{\mathrm{cut}} \sim 720$ nm, would still cover the infrared, millimeter, microwave, and rf domains. Thus the propagation of EMB's will be greatly sensitive to the material in which the propagation occurs. The EMB spectrum will be affected most strongly by metallic particles or any other good conductors (the part of the spectrum below the respective plasma frequency will be absorbed) or by the presence of water or other substances that have strong absorption bands, especially in the infrared. Designating the EMB radiation here S rays (where S stands for subcycle or subfemtosecond), in analogy to recently demonstrated T rays[10] (terahertz pulses; see below), we note that the fact that different materials have different transparencies for S rays suggests a great number of possible applications of EMB's to emulate x rays without x-ray-induced ionization damage. These S rays can be used, e.g., to monitor processing of high-density computer chips and for screening food products at food-processing facilities, luggage at airports, and concealed weapons. One can also envisage applications of S rays, similar to those for T rays but in the new frequency domain and with orders-of-magnitude broader spectra, for medical imaging, in particular, for a new kind of tomography, S tomography, with an additional possible advantage of positioning an S-ray source inside a human body. S rays can also be a useful tool as a diagnostic of high-density fusion plasmas.

This paper is structured as follows. Section 2 discusses a general relationship between the field and polarization, which results in a solitary wave as a solution of a full Maxwell equation plus arbitrary constitutive equations; Section 3 addresses an exact EMB solution of the full Maxwell–Bloch equation for a two-level system; Section 4 treats EMB's and shock waves that are due to a classical anharmonic potential with ionization; Section 5 discusses various approximate approaches to the transition processes in nonlinear EMB propagation; Section 6 concentrates on EMB generation by half-cycle pulses; Section 7 elaborates on multi-EMB solutions; Section 8 discusses shocklike wave fronts that are due to multi-EMB formation; and Section 9 gives an example of EMB formation by short laser pulses. Finally, we briefly discuss future research on, and physical ramifications of, EMB's.

2. MAXWELL EQUATIONS AND THE GENERAL SOLITARY-WAVE CONDITION

Maxwell's equation for the electric field **E** of a plane EM wave propagating along the z axis is

$$c^2 \partial^2 \mathbf{E}/\partial z^2 - \partial^2 \mathbf{E}/\partial t^2 = 4\pi \partial^2 \mathbf{P}/\partial t^2, \tag{2.1}$$

where $\mathbf{P}$ is the polarization density. Considering a pulse that propagates with a constant velocity $c\beta_{\mathrm{EMB}}$, introducing retarded variables $\tilde{t} \equiv t - z/\beta_{\mathrm{EMB}}c$ and $\tilde{z} = z$, and imposing a steady-state condition

$$\partial\mathbf{E}/\partial\tilde{z} = \partial\mathbf{P}/\partial\tilde{z} = 0, \tag{2.2}$$

we reduce Eq. (2.1) to the solitary-wave (EMB) Maxwell equation

$$\partial^2\mathbf{E}/\partial\tilde{t}^{\,2} = 4\pi M\partial^2\mathbf{P}/\partial\tilde{t}^{\,2}, \tag{2.3}$$

where

$$M \equiv \beta_{\mathrm{EMB}}{}^2(1 - \beta_{\mathrm{EMB}}{}^2)^{-1} = \text{const.}; \tag{2.4}$$

$\sqrt{M}$ is the normalized relativistic momentum of an EMB. Stipulating now that an EMB carries finite energy per unity area of cross section, i.e., that $\mathbf{E}, \mathbf{P} \to 0$ as $|\tilde{z}| \to \infty$ (a so-called bright soliton condition), and integrating Eq. (2.3) twice, we obtain a universal EMB-replication relationship between $\mathbf{E}$ and $\mathbf{P}$:

$$\mathbf{E}(\tilde{t}) = 4\pi M\mathbf{P}(\tilde{\mathbf{t}}). \tag{2.5}$$

Note that Eq. (2.5) is valid regardless of the constitutive relationship between $\mathbf{P}$ and $\mathbf{E}$. For our further calculations we assume that the field is linearly polarized, so that the wave equation can be reduced to a scalar equation, and introduce dimensionless variables: field f; polarization p; time $\tilde{\tau} = t\omega_0$, where ω_0 is a characteristic frequency of the system; and distance $\tilde{\zeta} = z\omega_0/c$; as well as a dimensionless particle density Q. All these variables and parameters are defined below for quantum and classical models separately; using them, we write the Maxwell equation as

$$\partial^2 f/\partial\tilde{\zeta}^{\,2} - \partial^2 f/\partial\tilde{\tau}^{\,2} = Q\partial^2 p/\partial\tilde{\tau}^{\,2} \tag{2.6}$$

and EMB-replication relationship (2.5) as

$$f(\tilde{\tau}) = QMp(\tilde{\tau}). \tag{2.7}$$

3. ELECTROMAGNETIC BUBBLES IN A TWO-LEVEL SYSTEM

Consider first pulse propagation in a medium of quantum TLS characterized by dipole moment $\mathbf{d}$ and resonant frequency ω_0. We introduce normalized variables: the field

$$f \equiv 2\mathbf{dE}/\hbar\omega_0 = 2\Omega_R/\omega_0, \qquad \Omega_R \equiv \mathbf{dE}/\hbar, \tag{3.1}$$

where Ω_R is the Rabi frequency; the polarization per atom $p = \rho_{12} + \rho_{21}$; the population difference per atom $\eta = \rho_{11} - \rho_{22}$, where ρ_{jk} $(j, k = 1, 2)$ are density-matrix elements of a TLS (with $\rho_{11} + \rho_{22} = 1$ and $\rho_{12} = \rho_{21}{}^*$); and time $\tau = (t - z/\beta_{\mathrm{EMB}}c)\omega_0$, to write full Bloch equations as

$$\dot{\eta} = -f\dot{p}, \qquad \ddot{p} + p = f\eta, \tag{3.2}$$

where the overdot designates $\partial/\partial\tau$. We use the notation of Ref. 19, which addresses generation of high harmonics in a superdressed TLS. Note that Eqs. (3.2) are not based on the rotating-wave approximation. Relaxation is not included in Eqs. (3.2) because we consider pulses much shorter than TLS relaxation times. The integral of the first of Eqs. (3.2) is square of the Rabi sphere radius:

$$\eta^2 + p^2 + \dot{p}^{\,2} = \text{const.} = 1. \tag{3.3}$$

The polarization density here is $\mathbf{P} = N\mathbf{d}p$, where N is the density of particles; therefore the parameter Q in Eq. (2.6) is

$$Q \equiv 4\alpha N\lambda_0(d/e)^2, \tag{3.4}$$

where e is the electron charge, $\lambda_0 = 2\pi c/\omega_0$, and $\alpha = e^2/\hbar c = 1/137$ is the fine-structure constant.

To find an EMB solution for TLS, we substitute condition (2.7) (with the unknown at this point M or β_{EMB}) into Eqs. (3.2). Having in mind the invariant (3.3) for atoms initially at equilibrium, $\eta \to 1$ at $|\tau| \to \infty$, such that the first of Eqs. (3.2) gives us $\eta(\tau) = 1 - f^2/(2QM)$, we obtain from the second of Eqs. (3.2) a nonlinear equation for the EMB field, $f(\tau)$:

$$\ddot{f} - f(QM - 1) + f^3/2 = 0, \tag{3.5}$$

which is a so-called Duffing equation. Its first integral is

$$\dot{f}^{\,2} = f^2(QM - 1) - f^4/4 + C \tag{3.6}$$

(the integration constant $C = 0$ under the bright-soliton condition), which determines a separatrix in the phase plane, $\dot{f}$ and f, starting and ending at the point $\dot{f} = f = 0$. The next integration gives us finally an EMB, a solitary, nonoscillating wave:

$$f(\tau) = \frac{f_{\mathrm{EMB}}}{\cosh(2\tau/\tau_{\mathrm{EMB}})}. \tag{3.7}$$

The polarization and the population are then, respectively,

$$p = f/QM, \qquad \eta(\tau) = 1 - fp/2. \tag{3.8}$$

In Eq. (3.7) the amplitude of EMB and its length are, respectively,

$$f_{\mathrm{EMB}} = 2\sqrt{QM - 1}, \qquad \tau_{\mathrm{EMB}} = 4/f_{\mathrm{EMB}}. \tag{3.9}$$

The dimensional EMB amplitude, E_{EMB}, by the definition of f [Eq. (3.1)], is

$$E_{\mathrm{EMB}} = f_{\mathrm{EMB}}\hbar\omega_0/2d = 2\hbar/t_{\mathrm{EMB}}d. \tag{3.10}$$

(For EMB length T, defined at a half-peak field, i.e., $T \approx t_{\mathrm{EMB}}/1.32 = \tau_{\mathrm{EMB}}/1.32\omega_0$, we have $E_{\mathrm{EMB}} = 1.32\hbar/Td$.)

Instead of having f_{EMB} as function of M or β_{EMB}, we can express β_{EMB} in terms of f_{EMB}:

$$\beta_{\mathrm{EMB}} = \sqrt{M/(1 + M)} = [1 + Q/(1 + f_{\mathrm{EMB}}{}^2/4)]^{-1/2} \tag{3.11}$$

or, if $Q \ll 1$ (Section 5 below),

$$\beta_{\mathrm{EMB}} \approx 1 - (Q/2)(1 + f_{\mathrm{EMB}}{}^2/4)^{-1}. \tag{3.12}$$

Shorter EMB's have higher amplitudes and move faster, approaching the vacuum speed of light. The lowest allowed speed of a bubble is

$$\beta_{\mathrm{LN}} = 1/\sqrt{1 + Q} \approx 1 - Q/2, \tag{3.13}$$

which corresponds to linear propagation of an adiabatically slow pulse.

The Fourier spectrum of EMB,

$$S_f(\omega) \propto 1/\cosh[\pi\omega/2(\Omega_R)_{\mathrm{peak}}], \tag{3.14}$$

spreads from zero to the cutoff frequency:

$$\omega_{\rm cut} \sim (\Omega_R)_{\rm peak} = dE_{\rm EMB}/\hbar. \tag{3.15}$$

Phase-portrait considerations show that, with $f = p = 1 - \eta = 0$ at $|\tau| \to \infty$, the nonoscillating EMB [Eq. (3.7)] is the only soliton supported by the system. Therefore, surprisingly, regular self-induced transparency envelope solitons,[1] which have been obtained in the rotating-wave approximation, are inconsistent with the exact solution [Eq. (3.7)] based on full Bloch equations (3.2). This indicates that higher-order approximations may render self-induced transparency solitons unstable at long enough distances. EMB (3.7) can be regarded as a full Bloch 2π soliton; by introducing phase (or area)

$$\phi_R(\tau) \equiv \int_{-\infty}^{\tau} f{\rm d}\tau \tag{3.16}$$

we get $\phi_R(\infty) = 2\pi$, which points to a full Bloch area theorem.

A similar EMB solution [Eq. (3.7)] holds also for amplifying TLS media with the inverse population, $\eta(|\tau| \to \infty) = -1$. In this case, however,[13]

$$\eta = -1 - fp/2, \qquad f_{\rm EMB} = (-QM - 1)^{1/2}, \qquad M < 0, \qquad \beta_{\rm EMB}{}^2 > 1. \tag{3.17}$$

Because a TLS with $\eta_\infty = -1$ is a nonequilibrium system storing pumping energy, $\beta_{\rm EMB}$ here is not the speed of energy propagation, so the fact that $\beta_{\rm EMB}{}^2 > 1$ (i.e., the EMB moves faster than light) is not incompatible with special relativity. More intense EMB's here move more slowly, approaching the speed of light from above as their amplitude increases.

4. ELECTROMAGNETIC BUBBLES AND SHOCK WAVES IN A CLASSICAL IONIZATION POTENTIAL

Solution (3.7) is valid within the limitations of our TLS model. In particular, the EMB duration, $t_{\rm EMB} = \tau_{\rm EMB}/\omega_0$, must be shorter that all the atomic relaxation times, which will still allow for EMB's as long as $\sim 10^{-9}$ s, with longer EMB's having a lower peak amplitude [Eqs. (3.8)] and moving more slowly [Eqs. (3.9)]. It is instructive to consider the example of xenon, with $\hbar\omega_0 \sim 8.44$ eV, effective dipole size $d/e \sim 0.7$ nm [based on the superdressed TLS data for high-harmonic generation in xenon (Ref. 19)], and $N \sim 10^{19}$ cm^{-3} ($Q \sim 10^{-2}$). For a 10-ps-long EMB we have $E_{\rm peak} \sim 10^3$ V/cm. Longer pulses can be considered within the TLS model with relaxation. Of particular interest, however, are the shortest and most intense pulses. When the EMB field approaches the atomic field ($\sim 10^8$–10^9 V/cm), the EMB formation is affected mainly by the atomic ionization potential, which limits EMB length and amplitude. For such fields, the TLS model is invalid. We can, however, evaluate limitations on EMB within a classical one-dimensional model of an atom with a strongly nonlinear potential, $U(x)$, limited at $|x| \to \infty$, to allow for ionization; here x is the electron displacement. Then Bloch equations (3.2) are replaced by a classical normalized equation for the electron motion:

$$\ddot{p} + {\rm d}u(p)/{\rm d}p = f(\tau), \tag{4.1}$$

with the dimensionless variables and parameters of the system defined as

$$f(\tau) \equiv eE(\tau)x_0/U_0, \qquad p \equiv x/x_0, \qquad \omega_0 = (U_0/m_e x_0{}^2)^{1/2}, \qquad Q = 4\pi N(ex_0)^2/U_0, \tag{4.2}$$

where x_0 is an atomic characteristic size and U_0 is a characteristic energy (e.g., the ionization potential)[20]; m_e is the electron mass. The polarization density here is $P = Nxe = Nex_0p$. Note that, for EMB's, TLS Bloch equations (3.2) reduce to a simple Duffing equation (e.g., for p):

$$\ddot{p} - Ap + Bp^3 = 0, \tag{4.3}$$

with $A = QM - 1$ and $B = (QM)^2/2$, which is equivalent to Eq. (4.1) (with $f = pMQ$) for the simplest classical anharmonic potential

$$u(p) = p^2/2 + ap^4, \qquad a = {\rm const.} > 0. \tag{4.4}$$

Hence the potential [Eq. (4.4)] can give rise to the same EMB [Eq. (3.7)]. For an arbitrary potential $u(p)$ the family of EMB solutions, $p(\tau)$, is found from Eq. (4.1) through the quadrature[13]

$$\int \{MQp^2 - 2[u(p) - u(0)]\}^{-1/2}{\rm d}p = \pm\tau. \tag{4.5}$$

A bright solitary solution to Eq. (4.5) exists, however, only for particular nonlinearities. For example, for Eq. (4.4) the nonlinearity must be positive, $a > 0$.[21] In general, if u is a smooth, monotonically increasing function of p^2, the bright solitary solution exists only if, near $p = 0$,

$$u(p) - u(0) > p^2{\rm d}u(0)/{\rm d}(p^2). \tag{4.6}$$

This condition requires that the atomic potential have sufficiently hard walls, which holds for some model potentials[22] [but not for a soft potential such as $u = -(1 + p^2)^{-1/2}$ (Ref. 22)]. An example of a model potential that allows for an explicit analytical solution of Eq. (4.5) is

$$u(p) = p^2(p^2 + b/2)/(1 + p^2)^2, \qquad b = {\rm const.} > 0. \tag{4.7}$$

To illustrate the limitations imposed by over-the-barrier ionization, we consider first a classical box potential, $u(p) = 0$ for $|p| < 1$ and $u(p) = 1$ otherwise, in which case the EMB field is

$$f(\tau) = f_{\rm EMB}\exp(-|\tau|\sqrt{f_{\rm EMB}}), \qquad f_{\rm EMB} \leqslant 2 \tag{4.8}$$

and $M = f_{\rm EMB}/Q$. (We presume here that an electron always starts its motion at $p = 0$.) Thus the maximal field strength $E_{\rm max}$ and the shortest EMB length $t_{\rm min}$ are

$$E_{\rm max} = U_0/ex_0, \qquad t_{\rm min} = (x_0/c)(m_e c^2/2U_0)^{1/2}, \tag{4.9}$$

where U_0 is an ionization limit and $2x_0$ is the total box width. $E_{\rm max}$ is of the same nature as an atomic field, $E_{\rm at} = E_{\rm max}/2$, i.e., the atom is ionized (in classical terms) by a pulse of a certain shape [here, Eq. (4.8)] if its peak amplitude exceeds $E_{\rm max}$; $t_{\rm min}$ is the time required for such a field to pull an electron out of the potential well. (With

$U_0 = 20$ eV and $x_0 = 0.1$ nm, $E_{\max} \approx 2\,10^9$ V/cm and $t_{\min} \sim 0.4\,10^{-16}$ s.) To make a connection to atoms with Coulomb long-range attraction, consider now a potential

$$u = 1 - (1 + 2bp^2 + p^4)^{-1/4}, \tag{4.10}$$

with $u - 1 \approx p^{-1}$ at $|p| \to \infty$. It has a single well and satisfies the hard-wall condition only when $0 \leqslant b \leqslant b_{\rm cr} = \sqrt{2/5}$. For a given U_0 and atomic number Z, we have

$$x_0 = r_e Z(m_e c^2/U_0),$$

$$\lambda_0 \equiv 2\pi c/\omega_0 = 2\pi r_e Z(m_e c^2/U_0)^{3/2}, \tag{4.11}$$

$$E_{\rm at} = (2/5)^{1/4} U_0/ex_0; \tag{4.12}$$

here $r_e = e^2/m_e c^2$ is the classic electron radius. As an illustration, consider a limiting case with $b = 0$. Small-amplitude EMB's are governed again by a Duffing equation, $\ddot{p} - MQp + p^3 \approx 0$, its solitary solution being $p \approx p_{\rm EMB}\sqrt{2}\ \mathrm{sech}(\tau p_{\rm EMB})$ (Fig. 1, curve 1). Here $p_{\rm EMB} = \sqrt{MQ}$, and therefore $\beta_{\rm cr} = 0$; i.e., small-amplitude EMB's here can move slowly, a typical feature of any potential with $\mathrm{d}u(0)/\mathrm{d}(p^2) = 0$. The EMB peak amplitude is $f_{\rm peak} = \sqrt{2(MQ)^3}$. Hence, as its amplitude increases, an EMB moves faster and shortens. However, at $p_{\rm peak} \approx (8/45)^{1/4} \approx 0.65$ and $f_{\rm peak} \approx 0.122$ the EMB length (at the half-peak amplitude) reaches its minimum, $\tau_{A\,\min} \approx 5.3$ (at the half-peak amplitude; Fig. 1, curve 2) or $\tau_{I\,\min} \approx 2$ (at the half-peak intensity). Assuming that $U_0 \approx 24$ eV and $Z = 2$, as in helium, one obtains the shortest EMB length:

$$t_{I\,\min} = 2(r_e Z/c)(m_e c^2/U_0)^{3/2} \sim 10^{-16}\ \text{s}. \tag{4.13}$$

(Significantly shorter EMB's can be attained with ionized atoms, e.g., ion beams, that may have an ionization potential U_0 orders of magnitude larger.) As the field amplitude continues to rise, EMB begins to broaden, becoming a flat-topped pulse (Fig. 1, curve 3). Finally, at a threshold amplitude, $p_{\rm peak} \approx 1.245$ and $f_{\rm peak} \approx 0.42$, it becomes a shock (antishock) wave whose single leading (trailing) edge is a front of an ionizing (deionizing) cw field (Fig. 1, curve 4).[23] The amplitude front rises (falls) as $\exp(\tau/\tau_{\rm ion})$, with $\tau_{\rm ion} \approx (MQ)^{-1/2} \approx 1.7$. This shock wave is typical of any hard-wall potential with ionization. Our preliminary results indicate, though, that a single-front shock wave becomes unstable, producing a short precursor that travels as a pilot EMB at a faster speed ahead of the group of other, longer, and closely spaced EMB's, which merge into a current-density field far behind the precursor. This pattern persists if one accounts for the plasma that is due to ionization behind the pilot group of EMB's. In a more detailed picture of a shock wave the classical over-the-barrier ionization near the threshold must be modified by quantum tunneling.

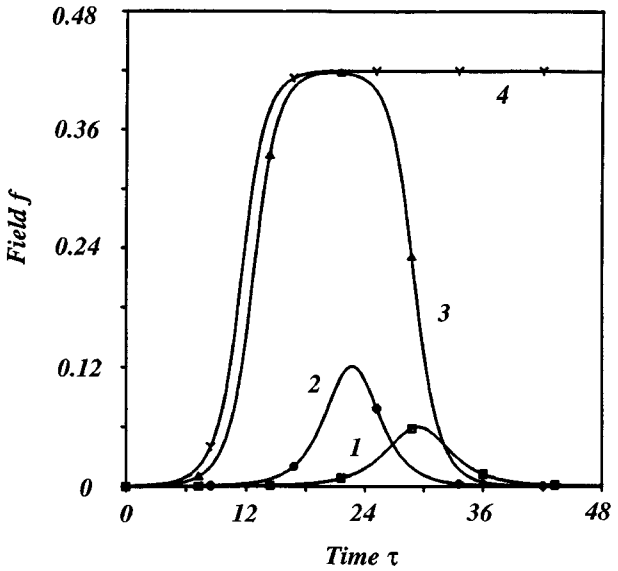

Fig. 1. Normalized field amplitude f versus time τ for steady-state EMB's (curves 1–3) and a shock wave (curve 4) due to ionization potential. Curve 1, $MQ = 0.12$; curve 2, $MQ = 0.187$; curve 3, $MQ = (MQ)_{\rm ion} - 10^{-5}$; curve 4, $MQ = (MQ)_{\rm ion} \approx 0.3403$.

5. VARIOUS APPROXIMATE APPROACHES TO ELECTROMAGNETIC BUBBLE PROPAGATION

To demonstrate the existence of EMB's (in both quantum and classical cases) most rigorously, we have used so far a double-full approach: full Maxwell equation (2.1) plus full constitutive equations (3.2) or (4.1) (i.e., without the rotating-wave approximation). The problem with this double-full approach is that at this point we do not have a mathematical theory that would allow us to handle a general solution of the problem (including the case of arbitrary initial–boundary conditions) with the same degree of confidence and insightfulness as the one provided by the inverse scattering theory for the so-called fully integrable partial differential equations, such as Kortdeweg–de Vries, nonlinear Schrödinger, and some other equations. There are no results regarding the full integrability of double-full equations or even about their being of the same class of equations that can lend themselves to the inverse scattering theory. In physical terms, the very fact that the full nonlinear Maxwell equation allows for coupling between forward- and backward-propagating waves creates a significant complicating factor. Hence, in a theoretical consideration of the propagation as well as in numerical simulations, particularly for all kinds of transient problems, we need to look for connections to some better understood equations, at least in certain meaningful limits. Closer consideration shows, fortunately, that double-full equations can often be reduced to much simpler equations (with some of them being fully integrable) while being kept free from a rotating-wave approximation and hence open to broad-spectrum solutions.

Our computer simulations have shown that at low density, $Q \ll 1$ (e.g., in gases, where typically $Q \sim 10^{-4}$–10^{-1}), the Maxwell equation can be reduced to an approximate first-order equation without loss of any significant feature of nonlinear propagation. In particular, the EMB solution has the same form as for a full Maxwell equation. This is explained by the fact that, when $Q \ll 1$, the propagation velocity approaches the speed of light, $1 - \beta = O(Q) \ll 1$, and any retroreflection can be neglected. Assuming now that the wave propa-

gates in only one direction (e.g., positive $\tilde{\zeta}$), using retarded variable $\tau = \tilde{\tau} - \tilde{\zeta}/\beta_{\mathrm{LN}}$, and keeping in mind definition (3.13), we transform Maxwell equation (2.6) into the equation

$$-\frac{\partial^2 f}{\partial \tilde{\zeta}^2} + \frac{2}{\beta_{\mathrm{LN}}}\frac{\partial^2 f}{\partial \tilde{\zeta}\partial \tau} = Q\frac{\partial^2 (f-p)}{\partial \tau^2}. \tag{5.1}$$

Neglecting in Eq. (5.1) the term $\partial^2 f/\partial \tilde{\zeta}^2$ (which is small because the pulse changes relatively slowly as it propagates along the $\tilde{\zeta}$ axis) and eliminating one derivative, $\partial/\partial\tau$, by integrating the resulting equation over $\partial\tau$, we can now write

$$\partial f/\partial \tilde{\zeta} = (Q\beta_{\mathrm{LN}}/2) \times [\partial(f-p)/\partial\tau]. \tag{5.2}$$

By rescaling the propagation coordinate, $\zeta \equiv \tilde{\zeta} Q \beta_{\mathrm{LN}}/2$, we finally obtain

$$\partial f/\partial \zeta = \partial(f-p)/\partial\tau. \tag{5.3}$$

The physical implication here is that nonlinear retroreflection is neglected; the counterpropagating waves are decoupled. We can verify the validity of the reduced Maxwell equation by using it instead of Eq. (2.6) to obtain EMB's in either quantum and classical limits as well as by numerical simulations of the transient propagation.[14,17] We also found that Eq. (5.3) can be used even if Q is not small, if the field spectrum does not stretch beyond ω_0.

To describe the studied process by even simpler equations, and especially by fully integrable ones, we can work now on the simplification of constitutive equations. A major step in this direction is based on the observation that, for most nonlinear gases of interest, in particular, for noble gases, the TLS frequency of the first transition, ω_0, is extremely high, so even near-femtosecond pulses and laser oscillations are relatively slow compared with a cycle of that frequency. How slow is "slow" in this case? Xenon has the lowest energy, $\mathscr{E}_0 = \hbar\omega_0$, of the first excited level among the noble atoms; with $\mathscr{E}_0 \sim 8.5$ eV, one cycle of ω_0 is $2\pi/\omega_0 \sim 0.5$ fs. For helium with $\mathscr{E}_0 \sim 20$ eV, one cycle is $\sim$0.2 fs. For any available HCP, the HCP length, t_0, is 3 orders of magnitude longer; even the full cycle of Ti:sapphire laser oscillation is $\sim$2.7 fs, which is still much longer than $2\pi/\omega_0$ in these gases. Another important parameter is the dimensionless amplitude of the incident field f_0, [Eq. (3.1)], which is also related to the time scale of the nonlinear motion in a TLS, $f_0 = O(\tau_{\mathrm{EMB}}^{-1})$. Thus, introducing a parameter $\varepsilon \equiv \tau_0^{-1} + |f_0|$, we can see that it is very small for HCP's available now or in the foreseeable future. For noble gases, for example, and with $E_0 \sim 2$ MV/cm, which is an order of magnitude higher than HCP's now available, we have $f_0 \sim 10^{-2}$; with $t_0 \sim 400$ fs we also have $\tau_0^{-1} \sim 10^{-3}$. Hence, if $\varepsilon \ll 1$, we can use a slow motion (but no envelopes) approximation whereby $f(\tau)$, $p(\tau)$, and $\eta(\tau)$ have their Fourier frequencies much smaller than ω_0. As a first-step, instantaneous weak response, we neglect $\ddot{p}$ in the second of Eqs. (3.2), so $p_1 = f\eta$, and substitute it into the first of Eqs. (3.2). By integrating the rewritten equation and having in mind the invariant [Eq. (3.3)] (i.e., $\eta = 1$ at $p = \dot{p} = 0$), we obtain

$$\eta_1 = (1+f^2)^{-1/2}, \qquad p_1 = f(1+f^2)^{-1/2}. \tag{5.4}$$

Writing $p = p_1 + \Delta p$ and $\eta = \eta_1 + \Delta\eta$ and neglecting again $\Delta\ddot{p}$ in [Eqs. (3.2)], by assuming now that $\ddot{p} \approx \ddot{p}_1$ we obtain, in the next approximation, $\Delta p \approx f\Delta\eta - \ddot{p}_1$, $\Delta\dot{\eta} \approx -f\Delta\dot{p}$. This relation, after we evaluate $\Delta\dot{p}$ from the latter of Eqs. (5.4) and substitute it into the former one, results in $\Delta\dot{\eta}(1+f^2) + f\dot{f}\eta = f(\mathrm{d}^3 p_1/\mathrm{d}\tau^3)$, integration of which yields $\Delta\eta \approx (p_1\ddot{p}_1 - \dot{p}_1^2/2)\eta_1$, $\Delta p \approx -p_1\eta_1^2 - p_1\dot{p}_1^2/2$. For $f-p$ we now have

$$f - p \approx p_1^3 \eta_1^{-1}(1+\eta_1)^{-1} + \ddot{p}_1\eta_1^2 + p_1\dot{p}_1^2/2. \tag{5.5}$$

The two last terms on the right-hand side of relation (5.5) reflect the Rabi dynamics without which EMB's would not exist. The right-hand side of relation (5.5) is $O(\varepsilon^3)$; the next approximation correction is $O(\varepsilon^5)$. In the limit $\varepsilon \to 0$, relation (5.5) can be further simplified when we notice that, because $\eta_1 = 1 - O(\varepsilon^2)$ and $\ddot{p}_1 = O(\varepsilon^3)$ as well as $\ddot{p}_1 = \ddot{f} + O(\varepsilon^5)$ and $p_1\dot{p}_1^2 = O(\varepsilon^5)$, we can write, still with the precision of $O(\varepsilon^5)$,

$$f - p \approx f^3/2 + \ddot{f}. \tag{5.6}$$

Relations (5.3) and (5.6) yield a single self-contained abridged Maxwell–Bloch equation:

$$\partial f/\partial\zeta - (3/2)f^2\partial f/\partial\tau - \partial^3 f/\partial\tau^3 = 0. \tag{5.7}$$

It can readily be shown that solution (3.7) of the full Maxwell–Bloch equations is also a solution of Eq. (5.7), which is one of the so-called modified Kortdeweg–de Vries (MKdV) equations. The MKdV solutions can be associated[24] with a normal Kortdeweg–de Vries equation, for which in the second term, instead of f^2, one has f. A MKdV equation is fully integrable by the inverse scattering method and has an infinite number of invariants.[24]

A similar equation can be obtained for a classical anharmonic oscillator [Eq. (4.1)] if the amplitude is not large, i.e., when approximation (4.4) with the coefficient of first-order nonlinearity, α, can be used. In this case, as for relation (5.6), we can write

$$f - p \approx 4af^3 + \ddot{f}, \tag{5.8}$$

and the self-contained wave equation, similar to Eq. (5.7), will again be the MKdV equation:

$$\partial f/\partial\zeta - 12af^2\partial f/\partial\tau - \partial^3 f/\partial\tau^3 = 0. \tag{5.9}$$

If the incident field is due to a laser and is, therefore, oscillating and strong, we may have $\varepsilon \gg 1$. Assuming that the TLS model and Bloch equations (3.2) are still valid, the Maxwell–Bloch equations can be reduced to another well-explored equation. Because we expect the driven polarization p to vary rapidly, we can drop p from the second of Eqs. (3.2), assuming that $\ddot{p} \gg p$. Solving Eqs. (3.2) in this approximation, we readily obtain

$$\dot{p} = \sin\phi_R, \quad \eta = \cos\phi_R, \tag{5.10}$$

where ϕ_R is the Rabi phase [Eq. (3.16)]; in this approximation $\dot{p}^2 + \eta^2 \approx 1$. Reduced Maxwell equation (5.3) can then be written as $\partial f/\partial\zeta - \partial f/\partial\tau = \sin\phi_R$ or as

$$\partial^2\phi_R/\partial\zeta\partial\tau - \partial^2\phi_R/\partial\tau^2 = \sin\phi_R. \tag{5.11}$$

With a proper choice of retarded coordinate τ_1, Eq. (5.11) can be reduced to an even simpler equation:

$$\partial^2 \phi_R / \partial \zeta \partial \tau_1 = \sin \phi_R . \tag{5.12}$$

These are different forms of the so-called sine-Gordon equation, which is fully integrable. It has again the same soliton solution, Eq. (3.7), as the general Maxwell–Bloch equations do. While using Eqs. (5.10)–(5.12), one has to be cautious about choosing boundary conditions; only those functions $f(\tau)$ at $\zeta = 0$ that satisfy a condition on the area of the pulse (see below), $S \equiv \phi_R(\infty) = 2\pi n$, where n is an integer, are applicable for simulations. (The best choice would be $S = 0$, because it would allow one to vary the amplitude of the incident field once the shape of the field is chosen.) If S is not an integer of 2π, this approximation will be inconsistent with the physics in the sense that neither area $S(\zeta)$ of the propagating pulse nor its energy W may be an invariant. Fortunately, the condition $S = 0$ can easily be satisfied for an oscillating field, which is exactly the area of the intended applicability of Eqs. (5.10)–(5.12). However, even more stringent conditions may be imposed by the fact that the TLS model is invalid when the Rabi frequency Ω_R exceeds the TLS frequency ω_0, i.e., when $f \gg 1$. Some other approximations that result in fully integrable equations can be found in Refs. 14–16.

We have to note that at this point no mathematical proof exists that in the general, double-full, formulation, EMB's are real solitons in the sense of full integrability of the full Maxwell plus full constitutive equations and that, therefore, EMB's are absolutely stable. Our numerical simulations for both TLS and nonlinear classical potentials show that small EMB's that are due to reduced Maxwell equation (5.3) are stable against both small and large (e.g., collision with another EMB) perturbations, which is consistent with the results of Ref. 14 for a TLS. Large EMB's (approaching the ionization threshold) may become unstable and break down into smaller EMB's. In a related simulation we discovered that significantly below the ionization threshold the EMB's are remarkably stable on temporal or spatial changes of medium parameters. In particular, when the gas density N was changed by 2 orders of magnitude along the path of propagation, the EMB profile and its length remained stable; only its velocity, β_{EMB}, was adjusting to a varying density, such that

$$N(z) M(\beta_{\mathrm{EMB}}) = \text{invariant}. \tag{5.13}$$

An EMB generated in a gas jet, for example, can therefore slide into vacuum without distortion.

Finally, it is worth noting that an interesting recent paper[25] suggested generation of nonoscillating or unipolar EM solitons and shocklike waves in nonlinear dielectrics as a result of the collective effect (phonons) in a crystal lattice. The time scale of these solutions is much larger than those discussed here, with the soliton length t_p much longer than a cycle of the transverse optic lattice's resonant frequency, ω_{OT}; i.e., $t_p \ll \omega_{\mathrm{OT}}{}^{-1}$; t_p would be no shorter than a few picoseconds for the best of materials. The nonlinearity in Ref. 25 scales as E^2, with the single soliton having a profile of $\cosh^{-2}$; the important fact is that, as shown in Ref. 25, the full nonlinear Maxwell equation for the case under consideration (based on a simplified constitutive equation that uses the assumption of low frequencies and a relatively weak field) can be reduced to a fully integrable Boussinesq-like equation.

6. ELECTROMAGNETIC BUBBLE GENERATION BY HALF-CYCLE PULSES

One of the major ways to generate EMB's[13] is to use existing HCP's[7–11] to launch much shorter EMB pulses in a nonlinear medium by means of a transient propagation process. It is important initially to obtain 50-fs to ~5-fs-long EMB's and thus to attain 1–2 orders of magnitude enhancement over available HCP's. In our computer simulations[13,17] we found that distinct individual EMB's could be obtained with a HCP. In these simulations we used incident HCP's [i.e., the solution $f(\zeta, \tau)$ at $\zeta = 0$] of various profiles that resembled a typical experimental profile, in particular, a Gaussian one:

$$f(\tau) \propto \exp[-(2\tau/\tau_0)^2], \tag{6.1}$$

and 1/cosh profile, i.e., the same as that of an EMB [Eq. (3.7)] but with its amplitude f_0 unrelated to its length τ_0:

$$f(\tau) = f_0 / \cosh(2\tau/\tau_0). \tag{6.2}$$

These profiles all show similar behavior in the formation of EMB's; in this paper we address 1/cosh profile (6.2) as the only one that can produce exact analytical results related to the formation of multiple EMB's; however, most of our results on the parameters of the leading (largest and fastest) EMB, the EMB precursor, particularly its amplitude, length, and formation distance, will be valid for any incident HCP. The TLS approximation is valid with great margin if the instantaneous Rabi frequency is relatively small, $f \ll 1$, which, as was shown in Section 5, is the case for the available HCP's; for instance, in noble gases, even with still unavailable $E = 2$ MV/cm, $f \sim 10^{-2}$.

For a given length of the incident HCP τ_0, the threshold (minimal) amplitude required for the HCP to attain a single EMB, provided that the HCP has the profile of Eq. (6.2), according to Eqs. (3.9) and (3.10) is

$$f_{\mathrm{thr}} = 4/\tau_0 \quad \text{or} \quad E_{\mathrm{thr}} = 2\hbar/t_0 d. \tag{6.3}$$

In most of our runs we used $\tau_0 = 4000$, which corresponds to $t_0 \sim 313$ fs (or to $t_0 = 413$ fs at the pulse's half-amplitude) for xenon [$\hbar\omega_0 \approx 8.5$ eV and $d/e \approx 0.7$ nm (Refs. 13 and 17)]; in this case $f_{\mathrm{thr}} = 10^{-3}$ and $E_{\mathrm{thr}} \approx 60$ KV/cm.

Typical patterns of EMB formation are shown in Figs. 2 and 3. Figure 2 depicts a double-EMB formation for $f_0 = 2 f_{\mathrm{thr}}$ [the larger EMB here is $3 f_{\mathrm{thr}} = (3/2) f_0 \rightarrow 180$ KV/cm] and for the weaker one, f_{thr}; they are, respectively, 104 and 313 fs long. Figure 2 can also be seen as a collision of two EMB's, with each of them coming out unaffected by the collision (aside from a slight shift of their center lines of propagation); this effect can be shown by retracing the plot back in $\zeta < 0$. For larger f_0, more EMB's are formed, and the strongest EMB moves faster than the rest of the pack, leading the train as a precursor. A density plot showing the linear trails of individual EMB's moving with different velocities, with

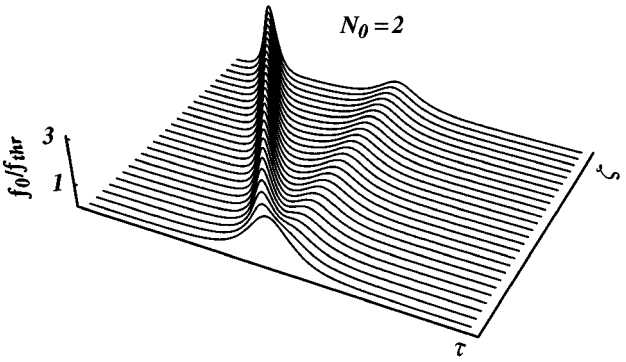

Fig. 2. Double-EMB formation by a HCP with $f_0 = 2 f_{\rm thr}$.

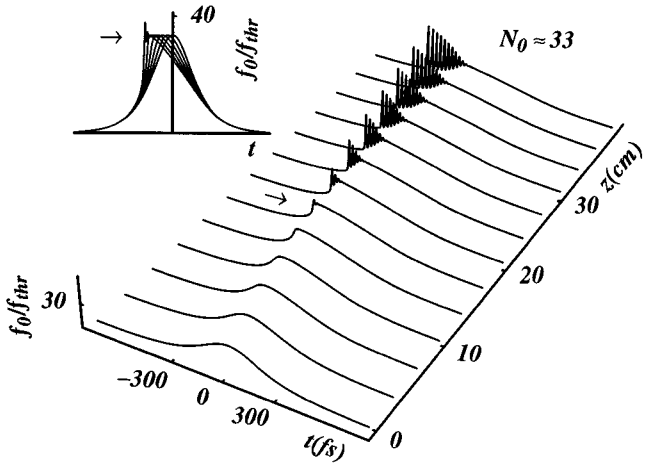

Fig. 3. Formation of multi-EMB's and a shocklike wave front for $f_0 f_{\rm thr}^{-1} \approx 33$ as the wave propagates in ζ; inset, superposition of the field profiles at different ζ, illustrating the front formation.

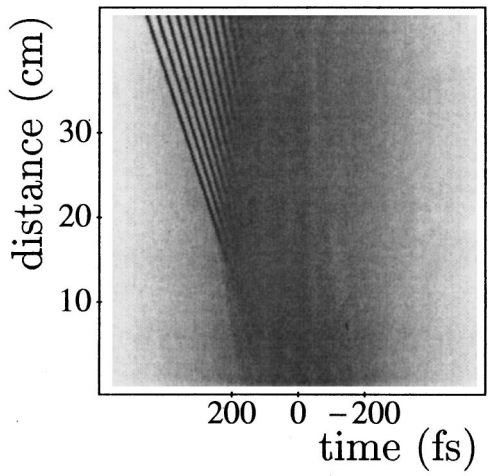

Fig. 4. Density plot for the propagation shown in Fig. 3; note that the trails of individual EMB's make straight lines; i.e., each of them propagates with its individual constant velocity $\beta_{\rm EMB}$ [Eq. (3.11)].

the front trail being due to the EMB precursor, is depicted in Fig. 4. As f_0 increases, the precursor grows stronger and shorter, and the distance $\zeta_{\rm EMB}$ for it to break away from the mother HCP decreases. Figure 3 depicts multi-EMB formation for $E_0 = 2$ MV/cm ($f_0 = 3.3 \times 10^{-2} = 33 f_{\rm thr}$), which is expected to be possible in the near future. In this case $z_{\rm EMB}$ is estimated (see the end of Section 8 below) from $\zeta_{\rm EMB} \sim 1.23 \times 10^5$; for xenon at 10 atm ($Q \sim 0.57$), it is $z_{\rm EMB} \sim 12.5\,cm$. The precursor here is 4.8 fs long, 2 orders of magnitude shorter than available HCP's.

In terms of experiment and application it is important to know how the properties of EMB's are controlled by the incident HCP. In this respect one has to answer a few important questions. Given the amplitude E_0 and the length t_0 of the incident HCP, what are the amplitude and the length of the leading EMB; how many EMB's (per HCP) can be generated, and what are the amplitudes and lengths of those EMB's; and what is the formation distance for the first EMB? Although the equations that govern the wave propagation are fully integrable in certain approximations (see Section 5), these questions cannot in general be answered analytically. Our combined numerical and analytical efforts[17] allowed us, however, to obtain remarkably simple results, which can be summarized as follows: The amplitude of the EMB, $E_{\rm EMB}$, is proportional to (and larger than) the amplitude E_0 of an incident HCP; the EMB's length is inversely proportional to $E_{\rm EMB}$; the number of the EMB's is proportional to the area of the incident HCP. We have also discovered that, when multiple EMB's are generated, at some point they form a shocklike wave front, whose formation is proportional to ${E_0}^{-2}$. We have shown that the distance of the first EMB formation is proportional to ${E_0}^{-3}$ if E_0 is relatively small; for sufficiently large E_0, this process coincides with the formation of a shocklike wave. The main good news is that short EMB's can be generated by a long HCP with a sufficiently large amplitude.

In our computer simulations[17] using HCP's of various profiles {in particular, Gaussian [(relation) (6.1)] and $\cosh^{-1}$ [Eq. (6.2)]}, we found that an EMB precursor shows a linear dependence of its amplitude, $f_{\rm EMB}$, on the incident amplitude, f_0, regardless of the profile:

$$f_{\rm EMB} \approx a f_0 - (a-1) f_{\rm thr}, \quad a = \text{const.} \sim 2. \tag{6.4}$$

For the profile [Eq. (6.2)], relation (6.4) becomes exact with $a = 2$, so

$$f_{\rm EMB} = 2 f_0 - f_{\rm thr}; \tag{6.5}$$

see Fig. 5. This result also gives the precursor's length:

$$\tau_{\rm EMB} \approx 4/(2 f_0 - f_{\rm thr}) = 2\tau_0/(\tau_0 f_0 - 2). \tag{6.6}$$

From expressions (6.5) and (6.6), the amplitude and the length of the largest EMB tend to constants as the HCP's length τ_0 increases (Fig. 6). Hence, to attain large and short EMB, there is no need to use a short incident pulse; the only prerequisite is a sufficiently high amplitude.

To explain these results and to find other characteristics of the EMB's, particularly their formation distance, we use here an approach reminiscent of that developed in the theory of modulation instability in self-focusing and in propagation of pulses in nonlinear optical fibers. Approximating an initially long and smooth HCP by an almost dc wave with the amplitude of the incident slow pulse, and evaluating the propagation characteristics of this wave, we analyze the behavior of small perturbations of this wave. Linearizing the original equations with re-

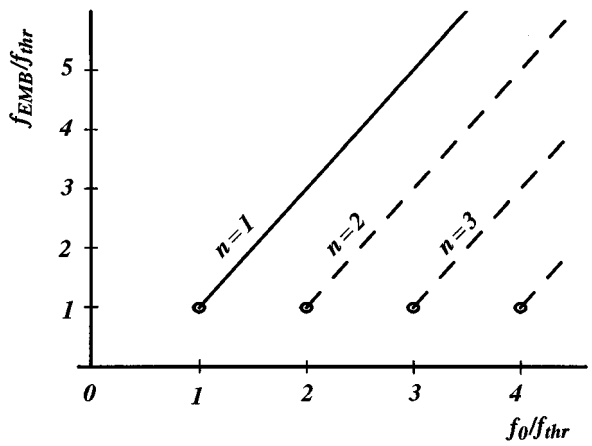

Fig. 5. EMB amplitude f_{EMB} versus amplitude f_0 of the incident HCP (both normalized to f_{thr}). Solid curve, EMB precursor; dashed curves, higher-order EMB's.

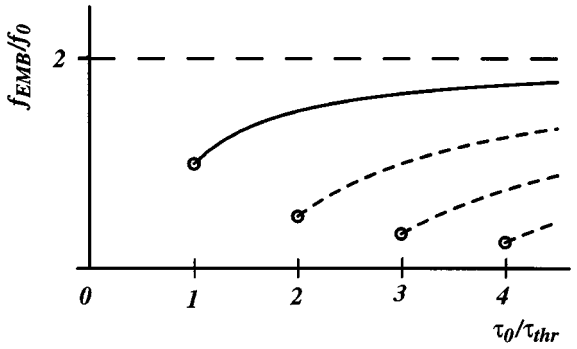

Fig. 6. EMB amplitude f_{EMB} versus length τ_0 of the incident HCP (normalized to f_{thr} and τ_{thr}, respectively). Solid curve, EMB precursor; dashed curves, higher-order EMB's.

spect to these perturbations, and deriving a dispersion equation for their spectral components, we then find the spectral component with the fastest phase change. The speed of propagation of this unique component, its frequency, and the spatial scale (the shortest of all the components) at which a sufficient phase accumulation occurs all point to an EMB precursor that will develop from this component.

Note that with this approach we can still work with full Maxwell plus constitutive equations; to demonstrate it, we show here how meaningful results can be obtained for full Maxwell–Bloch equations (2.6) and (3.2); we also keep track of simplifications that stem from reduced equations (5.3) and (5.7) and relation (5.6). Assuming a field with amplitude $f_0 =$ constant in Eqs. (2.6) and (3.2), we obtain that the population difference, polarization per atom, momentum parameter, and speed of this dc field are, respectively,

$$\eta_0 = \Omega_{\mathrm{ST}}{}^{-1}, \qquad p_0 = f_0\Omega_{\mathrm{ST}}{}^{-1},$$
$$QM_0 = \Omega_{\mathrm{ST}}, \qquad \beta_0 = (1 + Q\Omega_{\mathrm{ST}}{}^{-1})^{-1/2}, \tag{6.7}$$

where

$$\Omega_{\mathrm{ST}} \equiv (1 + f_0{}^2)^{1/2} \tag{6.8}$$

is the Stark-shifted frequency of the TLS that is due to the field effect. Now solving Eqs. (2.6) and (3.2) for small perturbations of this solution, and representing these perturbations in terms of spectral components $\exp[i(q\tilde{\zeta} - \Omega\tau)]$, we obtain the dispersion relationship between the wave number of the perturbation component q and its frequency Ω:

$$q = \Omega[1 + Q/\Omega_{\mathrm{ST}}(\Omega_{\mathrm{ST}}{}^2 - \Omega^2)]^{1/2}. \tag{6.9}$$

In the linear ($f_0 \to 0$), low-frequency ($\Omega \to 0$) limit we have

$$q_{\mathrm{LN}} = \Omega(1 + Q)^{1/2}. \tag{6.10}$$

The part of q that is due to both the nonlinearity and the dispersion if $Q \ll 1$ is thus

$$\Delta q \equiv q - q_{\mathrm{LN}} \approx (Q\Omega/2)[\Omega_{\mathrm{ST}}(\Omega_{\mathrm{ST}}{}^2 - \Omega^2)^{-1} - 1]. \tag{6.11}$$

The lowest $\Delta q(\Omega) < 0$ corresponds to the fastest perturbation. Looking for the minimum of Δq, we obtain the frequency, $\Omega = \Omega_{\mathrm{fast}}$, of this component as

$$(\Omega_{\mathrm{fast}}/\Omega_{\mathrm{ST}})^2 = [2\Omega_{\mathrm{ST}}{}^3 + 1 - (8\Omega_{\mathrm{ST}}{}^3 + 1)]^{1/2}/2\Omega_{\mathrm{ST}}{}^3; \tag{6.12}$$

hence, if $f_0{}^2 \ll 1$, we have

$$\Omega_{\mathrm{fast}} \approx f_0{}^2/2. \tag{6.13}$$

Substituting $\Omega = \Omega_{\mathrm{fast}}$ into Eq. (6.9), we evaluate q_{fast} and the phase velocity $\beta_{\mathrm{fast}} \equiv \Omega_{\mathrm{fast}}/q_{\mathrm{fast}}$ of this component in the case $Q \ll 1$ as

$$\beta_{\mathrm{fast}} \approx 1 - Q/[1 + (8\Omega_{\mathrm{ST}}{}^3 + 1)^{1/2}]. \tag{6.14}$$

Comparison with Eq. (3.11) shows that a matching EMB, $\beta_{\mathrm{EMB}} = \beta_{\mathrm{fast}}$, has an amplitude

$$f_{\mathrm{fast}} = \{2[(8\Omega_{\mathrm{ST}}{}^3 + 1)^{1/2} - 3]\}^{1/2} \tag{6.15}$$

or, for $f_0{}^2 \ll 1$,[17]

$$f_{\mathrm{fast}} \approx 2f_0. \tag{6.16}$$

Equation (6.16) confirms the linear dependence between f_0 and f_{fast} in relation (6.4) and perfectly fits the coefficient $a = 2$ in Eq. (6.5). Note that, in an ideal dc field, $\tau_0 \to \infty$ and thus $f_{\mathrm{thr}} \to 0$, which explains the difference between Eq. (6.5) and relation (6.16).

The same approach can be used to estimate the precursor formation distance $\tilde{\zeta}_{\mathrm{EMB}}$, but only in the limited range of the parameters, because in general $\tilde{\zeta}_{\mathrm{EMB}}$ depends on the total area of the HCP (see below). To continue to use the perturbation approach we again substitute $\Omega = \Omega_{\mathrm{fast}}$ into Eq. (6.9) and estimate $\tilde{\zeta}_{\mathrm{EMB}}$ as a distance at which a certain change of phase, $\phi = 0(2\pi)$, is accumulated (the best fit is provided by $\phi = \pi\sqrt{10}$). In particular, if $f_0 \ll 1$, $\Delta q_{\mathrm{fast}} \approx -Qf_0{}^3/\sqrt{2}$ and[17]

$$\tilde{\zeta}_{\mathrm{EMB}} \sim \pi\sqrt{10}|\Delta q_{\mathrm{fast}}|^{-1} = 2\pi\sqrt{5}Q^{-1}f_0{}^{-3}$$
$$\text{or } \zeta_{\mathrm{EMB}} \sim \pi\sqrt{5}f_0{}^{-3} \tag{6.17}$$

(curve 1 in Fig. 7). Thus ζ_{EMB}, estimated by a phase change, scales as $f_0{}^{-3}$, which compares well with the distance of the first appearance of a saddle point, $\partial f/\partial\tau = \partial^2 f/\partial\tau^2 = 0$ (filled circles in Fig. 7), in the numerically obtained field profile up to $(f_0/f_{\mathrm{thr}})_{\mathrm{cr}} = N_{\mathrm{cr}}$

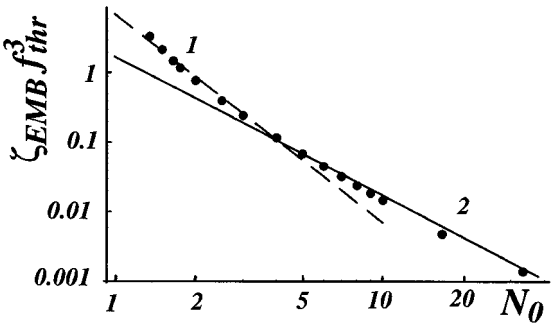

Fig. 7. Normalized formation distance $\zeta_{\mathrm{EMB}} f_{\mathrm{thr}}{}^3$ of an EMB precursor versus normalized incident amplitude $N_0 = f_0 f_{\mathrm{thr}}{}^{-1}$. Curve 1, $\pi\sqrt{5}N_0{}^{-3}$ [relation (6.17)]; curve 2, $\sqrt{3}N_0{}^{-2}$ [relation (6.18)]; filled circles, first saddle point appearance in a field profile.

$\sim$ 4. For larger f_0, when multiple EMB's are generated (see below), right before the EMB precursor breaks away, the initially smooth HCP drastically steepens to form a shocklike wave (Fig. 3), which, unlike a dc ionization shock wave (Section 4), can appear far below ionization. Its formation distance, ζ_{sh} (curve 2 in Fig. 7), which can be calculated analytically based on the theory of shocklike waves (Section 8 below), is[17]

$$\zeta_{\mathrm{sh}} \approx \zeta_{\mathrm{EMB}} \approx \sqrt{3}(f_0{}^2 f_{\mathrm{thr}})^{-1}, \qquad f_0 > 4f_{\mathrm{thr}}, \quad (6.18)$$

which scales as $f_0{}^{-2}$ now.

7. MULTIBUBBLE SOLUTION

When the incident amplitude of a HCP, f_0, sufficiently exceeds the threshold of EMB formation, f_{thr}, more than one EMB will be generated, as one can see from Figs. 2 and 3. In the limit $f_0 \ll 1$, when the propagation is described by MKdV equation (5.7), one can develop the analytical theory of N-bubble solutions for the profile of Eq. (6.2). The results of our theory are based on invariants of the MKdV equation[24] and are briefly summarized here. The total number of EMB's, N_{EMB}, is

$$N_{\mathrm{EMB}} = L(N_0), \qquad N_0 \equiv f_0 f_{\mathrm{thr}}{}^{-1} = f_0\tau_0/4, \quad (7.1)$$

where $L(x)$ is the largest integer not greater than x. For $N_0 \gg 1$, N_{EMB} is proportional to the incident HCP area, $f_0\tau_0$. With the EMB precursor designated 1, the amplitude f_n of the nth EMB is given by an amazingly simple formula:

$$f_n f_{\mathrm{thr}}{}^{-1} = 2(N_0 - n) + 1, \qquad n \leqslant N_0, \quad (7.2)$$

such that the decrement

$$f_{n-1} - f_n = 2f_{\mathrm{thr}} \quad (7.3)$$

is independent of n. Inasmuch as each bubble with amplitude f_{EMB} carries an energy

$$W_{\mathrm{EMB}} = f_{\mathrm{EMB}}^2 \tau_{\mathrm{EMB}} = 4f_{\mathrm{EMB}}, \quad (7.4)$$

which is proportional to its amplitude f_{EMB}, a unique quality of function (6.2) is that the energies of the bubbles generated by it are equidistant, or quantized, in a way reminiscent of the energy spectrum of a linear oscillator, where the quantum (or "quton") of their energy spectrum is $\Delta W_q = 2W_{\mathrm{thr}}$. It is worth noting that, when N_0 is an integer, the lowest energy of a bubble is exactly $W_{\mathrm{thr}} = \Delta W_q/2$, which again is reminiscent of the energy of the ground level of a linear oscillator, which is equal to half of the quantum of excitation.

For the EMB precursor, $n = 1$, Eq. (7.2) coincides with Eq. (6.5), as expected. If f_0 is an integer of f_{thr} [Eq. (6.3)], the incident HCP gives rise to an exact N-bubble solution. Otherwise a part, ΔW_{rad}, of its incident energy W_0 is radiated away into nontrapped modes whose relative effect decreases rapidly as the total number of EMB's increases:

$$\Delta W_{\mathrm{rad}} W_{\mathrm{thr}}{}^{-1} \equiv [N_0 - L(N_0)]^2 \leqslant 1. \quad (7.5)$$

Thus ΔW_{rad} is always smaller than the critical (smallest) energy W_{thr} of a bubble (for the fixed τ_0). Furthermore, as the incident amplitude increases, the relative maximum energy of untrapped radiation greatly decreases:

$$\Delta W_{\mathrm{rad}} W_0{}^{-1} \leqslant N_0{}^{-2}. \quad (7.6)$$

8. SHOCKLIKE WAVE FRONTS

When the incident HC-pulse is sufficiently strong to generate many EMB's ($N_0 \gg 1$), immediately before the EMB precursor is formed the initially smooth HCP drastically steepens and forms a shock wave at the front of the pulse. The formation of the EMB precursor coincides with the point in space at which the shock wave is steepest; this front is approximately τ_{EMB} long. After this point the shock wave breaks into the train of EMB's. To investigate this shock wave formation and estimate the location of the breaking point we make a further approximation, which can be called an instantaneous reaction, by dropping the higher derivative terms in the constitutive equations of the system. In the limit $Q \ll 1$, Eq. (5.3) is replaced in the case of a TLS by

$$\partial f/\partial\zeta = [1 - (1 + f^2)^{-3/2}]\partial f/\partial\tau; \quad (8.1)$$

and in the case of the anharmonic classical oscillator [Eq. (5.3)], by

$$\frac{\partial p}{\partial\tau} = \left(\frac{\partial}{\partial\zeta} - \frac{\partial}{\partial\tau}\right)\left(\frac{\mathrm{d}u}{\mathrm{d}p}\right). \quad (8.2)$$

If the HCP amplitude is small, $f \ll 1$, Eqs. (8.1) and (8.2) are further simplified to

$$\partial f/\partial\zeta = 12af^2\partial f/\partial\tau, \quad (8.3)$$

where a is the same as in Eq. (4.4) for classical anharmonic potential; $a = 1/8$ for a TLS. Any equation in the form

$$\partial f/\partial\zeta = F(f)\partial f/\partial\tau, \quad (8.4)$$

where $F(f)$ is some smooth function, has a general solution whereby each point of the solution, $f = f_1$, moves with the fixed velocity determined by f_1:

$$f[\tau + F(f_1)\zeta] = f_1, \quad (8.5)$$

where for Eq. (8.1) $F(f) = 1 - (1 + f^2)^{-3/2}$ and for Eq. (8.3) $F(f) = 12af^2$. Now, evaluating the derivative $\partial f/\partial\tau$ at point ζ, we find that

$$\frac{\partial f}{\partial \tau} = \frac{(\partial f/\partial \tau)_{\zeta=0}}{1 + \zeta(\mathrm{d}F/\mathrm{d}f)(\partial f/\partial \tau)_{\zeta=0}} = \frac{(\partial f/\partial \tau)_{\zeta=0}}{1 + \zeta(\partial F/\partial \tau)_{\zeta=0}} \tag{8.6}$$

such that for any nonzero $(\mathrm{d}F/\mathrm{d}f)(\partial f/\partial \tau)_{\zeta=0}$ there will be a point ζ at which $\partial f/\partial \tau \to \infty$, which signifies the formation of a shock wave. Because the formation of the shock wave will be arrested at amplitude f_1 at which $(\partial F/\partial \tau)_{\zeta=0}$ is maximal, we find that for profile (6.2) such a point is at $\cosh^2(2\tau/\tau_0) = 3/2$ or at $f = f_0\sqrt{2/3}$, with $[(\partial F/\partial \tau)_{\zeta=0}]_{\max} = -32af_0{}^2(\tau_0\sqrt{3})^{-1}$. Hence the distance of formation of the shock wave is

$$\zeta_{\mathrm{sh}} = -\frac{1}{[(\partial F/\partial \tau)_{\zeta=0}]_{\max}} = \frac{\tau_0\sqrt{3}}{32af_0{}^2}, \tag{8.7}$$

which in the case of a TLS (i.e., when $a = 1/8$ and $\tau_0 = 4/f_{\mathrm{thr}}$) gives relation (6.18). At the point of shock wave formation the full constitutive equation will prevent the discontinuity of the exact solution and break the shock wave into a train of solitons; the length of the steepest rise of the shock wave is thus determined by the EMB precursor time [Eqs. (3.9)].

Consider an example, $E_0 = 2$ MV/cm with $t_0 \sim 313$ fs (or 413 fs at pulse's half-amplitude), in xenon. In this case $f_{\mathrm{thr}} = 10^{-3}$ and $E_{\mathrm{thr}} \approx 60$ kV/cm ($f_0 \approx 3.3 \times 10^{-2} = 33f_{\mathrm{thr}}$), and the formation distance is estimated [relation (6.18)] as $\zeta_{\mathrm{EMB}} \sim 1.54 \times 10^6$, which under 10-atm pressure ($Q \sim 0.57$) translates into $z_{\mathrm{sh}} \sim 12.5$ cm. The EMB precursor here is 4.8 fs long, 2 orders of magnitude shorter than available HCP's. Note that in all these examples with HCP's the field $f \ll 1$ ($\Omega_R \ll \omega_0$) is much below the superdressed regime of a TLS and therefore far from the ionization.

The distance of the shock wave (and the first EMB) formation can be shortened if the wave's leading front is sharpened (e.g., by a shatter) such that $\tau_{\mathrm{lead}} < \tau_0$. We can then evaluate the distance ζ_{sh} by multiplying Eq. (8.7) by a factor $\tau_{\mathrm{lead}}/\tau_0$; in the above example, if the HCP leading front is shortened to ~40 fs the shock formation distance reduces to 1.25 cm.

9. ELECTROMAGNETIC BUBBLE GENERATION BY A SHORT LASER PULSE

Even the highest realistically expected fields of HCP's are still much lower that the amplitudes readily attainable in lasers. The possibility of EMB formation in each laser cycle, therefore, increases greatly, although the ensuing picture becomes more complicated because of the multiple EMB interactions, when regular laser radiation with many oscillations in the envelope is used instead of HCP's. Indeed, inasmuch as the laser cycle is much shorter (e.g., the cycle duration for the radiation with $\lambda = 0.9\ \mu$m is ~3 fs) with laser intensities of $\sim 10^{14}$ W/cm^2 (which corresponds to the field $\sim 2.7 \times 10^8$ V/cm), the EMB formation distance reduces to less than 1 mm and the EMB becomes an order of magnitude shorter than the optical cycle. Figure 8 shows a group of EMB's developing from a very short (6-fs) laser pulse with the relatively low peak intensity 6.8×10^{12} W/cm^2. One can see that the EMB formation length is approximately 0.1–0.2 mm and that the length of the EMB precursor is approximately 0.5 fs. There is a distinct possibility that the high-order harmonic generation[26] in noble gases might be attributed to a substantial degree to the multiple-EMB formation, which would explain many major features of the HHG phenomenon, such as its puzzling insensitivity to the phase mismatch at different high harmonics and the broadening and shift of harmonic spectra.

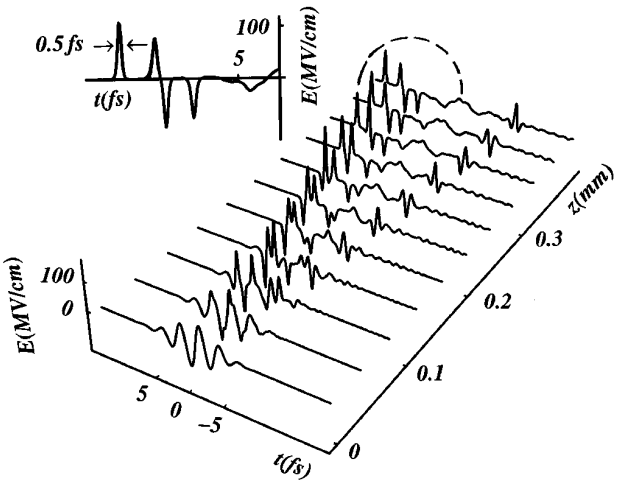

Fig. 8. EMB formation from an oscillating laser pulse ($t_p \approx 6$ fs). Inset, final cross section magnified to show EMB's.

10. CONCLUSION

In conclusion, we have theoretically demonstrated feasibility of powerful, near-femtosecond and subfemtosecond subcycle EM pulses and solitary waves, EM bubbles, supported by both quantum and classical nonlinear media. We have shown how their maximum amplitude and minimum length are limited by the atomic ionization. It follows from our theory that 10–0.1-fs EMB's can be generated by the available half-cycle pulses and short laser pulses; the peak EMB intensity can reach 10^{14}–10^{16} W/cm^2. Those results represent only the first steps in the exploration of the new time domain. Our hope is that EMB's will be experimentally observed in the near future. This realization will pose a new set of problems, such as EMB detection and characterization, separation, gating, control, focusing, and guiding, and exploration of various EMB applications. Further research should also consider two- and three-dimensional propagation; in a transverse-limited EM field a zero-frequency spectral component of the incident HCP will not propagate beyond the near-field area, and in the far-field area EMB will assume a modified profile.[27]

The new time domain, which is largely an uncharted territory, holds many promises for physics of field–matter interaction. The most familiar nonlinear effects and parameters associated with coherent light–matter interactions [harmonic generation, self-induced transparency, photon echoes, soliton generation and propagation, saturation of all kinds, n_2, $\chi^{(3)}$, etc.] are likely to take on entirely different forms or may even cease to exist. One of the most fundamental and intriguing phenomena is the field ionization of atoms, molecules, and semiconductor

quantum wells by a supershort pulse with an amplitude comparable with or larger than the ionization threshold. Such pulses could cause a substantial shake-up excitation or ionization of an atomic system within a time much shorter than any characteristic time of the system. In our most recent research, published elsewhere,[28] we show that a unipolar EMB a few femtoseconds long acting on a semiconductor quantum well can cause both forward and backward field ionization, with the photoelectrons emitted in both directions (i.e., not only in the direction of the ionizing unipolar field) with comparable intensities. Even more fundamental and exciting results are obtained for a hydrogen atom hit by a subcycle pulse with a subatomic unit amplitude. We have observed that the ionization response of the atom consists of a sequence of well-separated peaks resulting in strong spatiotemporal inhomogeneity of the photoelectron cloud and found an explanation for such a behavior.

ACKNOWLEDGMENTS

This research was supported by the U.S. Air Force Office of Scientific Research. The work by S. F. Straub is supported in part by the Deutsche Forschungsgemeinschaft. A. E. Kaplan is a recipient of the Alexander von Humboldt Award for Senior U.S. Scientists given by the Alexander von Humboldt Foundation of Germany.

S. F. Straub is also with the Abteilung für Quantenphysik, Ulm University, Ulm, Germany.

REFERENCES AND NOTES

1. S. L. McCall and E. L. Hahn, Phys. Rev. Lett. **18**, 908 (1967).
2. P. W. Smith, Proc. IEEE **1342**, 58 (1970), and references therein.
3. A. Hasegava and F. D. Tappert, Appl. Phys. Lett. **23**, 142 (1971).
4. V. E. Zakharov and A. B. Shabat, Sov. Phys. JETP **34**, 62 (1972).
5. R. L. Fork, C. H. Brito Cruz, P. C. Becker, and C. V. Shank, Opt. Lett. **12**, 483 (1987); M. Nisoli, S. de Silvestri, O. Svelto, R. Szipocs, K. Ferencz, C. Spielmann, S. Sartania, and F. Krausz, Opt. Lett. **22**, 522 (1997).
6. K. E. Oughstun and H. Xiao, Phys. Rev. Lett. **78**, 642 (1997); K. E. Oughstun and G. C. Sherman, *Electromagnetic Pulse Propagation in Causal Dielectrics* (Springer-Verlag, Berlin, 1994).
7. P. R. Smith, D. H. Auston, and M. S. Nuss, IEEE J. Quantum Electron. **24**, 255 (1988).
8. D. Grischkowsky, S. Keidin, M. van Exter, and Ch. Fattinger, J. Opt. Soc. Am. B **7**, 2006 (1990); R. A. Cheville and D. Grischkowsky, Opt. Lett. **20**, 1646 (1995).
9. J. H. Glownia, J. A. Misewich, and P. P. Sorokin, J. Chem. Phys. **92**, 3335 (1990).
10. B. B. Hu and M. S. Nuss, Opt. Lett. **20**, 1716 (1995).
11. R. R. Jones, D. You, and P. H. Bucksbaum, Phys. Rev. Lett. **70**, 1236 (1993); C. O. Reinhold, M. Melles, H. Shao, and J. Burgdorfer, J. Phys. B **26**, L659 (1993).
12. A. E. Kaplan, Phys. Rev. Lett. **73**, 1243 (1994); A. E. Kaplan and P. L. Shkolnikov, J. Opt. Soc. Am. B **13**, 412 (1996).
13. A. E. Kaplan and P. L. Shkolnikov, Phys. Rev. Lett. **75**, 2316 (1995); J. Nonlinear Opt. Phys. Mater. **4**, 831 (1995).
14. R. K. Bullough and F. Ahmad, Phys. Rev. Lett. **27**, 330 (1971); J. C. Eilbeck, J. D. Gibbon, P. J. Caudrey, and R. K. Bullough, J. Phys. A **6**, 1337 (1973).
15. E. M. Belenov, A. V. Nazarkin, and V. A. Ushchapovskii, Sov. Phys. JETP **73**, 423 (1991).
16. A. I. Maimistov, Opt. Spectrosc. (USSR) **76**, 569 (1994); **78**, 435 (1995).
17. A. E. Kaplan, S. F. Straub, and P. L. Shkolnikov, Opt. Lett. **22**, 405 (1997).
18. B. Kohler, V. Yakovlev, J. Ghe, M. Messina, K. R. Wilson, N. Schwentner, R. M. Whitnell, and Y. Yan, Phys. Rev. Lett. **74**, 3360 (1995).
19. A. E. Kaplan and P. L. Shkolnikov, Phys. Rev. A **49**, 1275 (1994).
20. For a harmonic oscillator with a frequency ω_0 it is natural to choose $U_0 = \hbar\omega_0$, with $x_0 = \sqrt{\lambda_C \lambda_0}$, where $\lambda_C = h/m_e c = 2.4 \times 10^{-2}$ Å is the Compton wavelength.
21. If nonlinearity is negative, $a < 0$, one can expect formation of dark a EMB (a solitary hole propagating on a static field background): $f(\tau) \propto f_0 \tanh(\tau f_0)$, $f_0 =$ constant.
22. D. G. Lappas, M. V. Fedorov, and J. H. Eberly, Phys. Rev. A **47**, 1327 (1993); J. H. Eberly, Q. Su, and J. Javanainen, J. Opt. Soc. Am. B **6**, 1289 (1989).
23. Recent studies of shocklike envelope fronts can be found, e.g., in S. R. Hartmann and J. T. Massanah, Opt. Lett. **16**, 1349 (1991); E. Hudis and A. E. Kaplan, Opt. Lett. **19**, 616 (1994); W. Forysiak, R. G. Flesh, J. V. Moloney, and E. M. Wright, Phys. Rev. Lett. **76**, 3695 (1996).
24. R. M. Miura, J. Math. Phys. **9**, 1202 (1968); R. M. Miura, C. S. Gardner, and M. D. Kruskal, J. Math. Phys. **9**, 1204 (1968); M. Wadati, J. Phys. Soc. Jpn. **32**, 1681 (1972); **34**, 1289 (1973).
25. L. Xu, D. H. Auston, and A. Hasegawa, Phys. Rev. A **45**, 3184 (1992).
26. A. McPherson, G. Gibson, H. Jara, U. Johann, T. S. Luk, I. A. McIntyre, K. Boyer, and C. K. Rhodes, J. Opt. Soc. Am. B **4**, 595 (1987); M. Ferray, A. L'Huillier, X. F. Li, L. A. Lompre, G. Mainfray, and C. Manus, J. Phys. B **21**, L31 (1988); A. L'Huillier and Ph. Balcou, Phys. Rev. Lett. **70**, 774 (1993); A. L'Huillier, L. A. Lompre, G. Mainfray, and C. Manus, in *Atoms in Intense Laser Fields*, M. Gavrila, ed. (Academic, Boston, Mass., 1992), pp. 139–206.
27. A. E. Kaplan, submitted to J. Opt. Soc. Am. B.
28. P. L. Shkolnikov, S. F. Straub, and A. E. Kaplan, in *Quantum Electronics and Laser Science Conference*, Vol. 12 of 1997 OSA Technical Digest Series (Optical Society of America, Washington, D.C., 1997), p. 31.